GMT systems define a new class of mobile elements rich in bacterial defensive and offensive tools

Tridib Mahata[1], Katarzyna Kanarek[1], Moran G. Goren[1], Rameshkumar Marimuthu Ragavan[1], Eran Bosis[2,*], Udi Qimron[1,*], & Dor Salomon[1,*]

[1] Department of Clinical Microbiology and Immunology, Faculty of Medicine, Tel Aviv University, Tel Aviv, Israel

[2] Department of Biotechnology Engineering, Braude College of Engineering, Karmiel, Israel

* For correspondence: EB, bosis@braude.ac.il; UQ, ehudq@tauex.tau.ac.il; DS, dorsalomon@mail.tau.ac.il

Keywords: T6SS, anti-phage, toxin, effector, antibacterial, nuclease, DNA mobility, integrase, GMT, Vibrio

Abstract

Conflicts between bacteria and their rivals led to an evolutionary arms race and the development of bacterial immune systems. Although diverse immunity mechanisms were recently identified, many remain unknown, and their dissemination within bacteria is poorly understood. Here, we describe a widespread genetic element, defined by the presence of the Gamma-Mobile-Trio (GMT) proteins, that serves as a bacterial survival kit. We show that GMT-containing genomic islands are active mobile elements with cargo comprising various antibacterial type VI secretion system (T6SS) effectors and anti-phage defense systems. We identify four new anti-phage defense systems encoded within GMT islands. A thorough investigation of one system reveals that it is triggered by a phage capsid protein to induce cell dormancy. Our findings underscore the need to broaden the concept of ‘defense islands’ to include also offensive tools, such as T6SS effectors, which we contend should be regarded as part of the bacterial immune system.

Introduction

Competition and predation contribute to bacterial evolution. For example, the type VI secretion system (T6SS), an offensive, missile-like dueling apparatus that delivers antibacterial toxins (i.e., effectors) directly into rival bacteria [1–5], was shown to shift the balance of bacterial populations and lead to the emergence of dominant strains [6–11]. Similarly, bacteriophages (hereafter referred to as phages) drive bacterial evolution and population dynamics [12–14]. Their ability to prey on bacteria has led to an arms race in which bacteria evolve or acquire anti-phage defense systems, while phages counteract these actions with anti-defense mechanisms [15]. Interestingly, anti-phage defense systems often cluster in so-called 'defense islands' [16,17], a phenomenon that has been used to identify dozens of diverse anti-phage defense systems in recent years [18–20]. Probably, many defense systems are yet to be revealed.

Mobile genetic elements (MGEs), such as plasmids, phages, and transposable elements, mediate horizontal gene transfer (HGT) and play a significant role in bacterial evolution [21–23]. They contain important information that can enhance bacterial fitness [24–27]. Anti-phage defense systems and secreted antibacterial toxins have been identified within MGEs and were predicted to be horizontally shared [13,20,28–34]. Nevertheless, many MGEs are poorly understood and require further investigation to reveal their distribution mechanisms and cargo.

We previously reported that *Vibrio parahaemolyticus* island-6 (VPaI-6), a genomic island encompassing *vpa1270-vpa1254* in the human pathogen *V. parahaemolyticus* RIMD 2210633 (hereafter referred to as RIMD) [35], encodes an antibacterial DNase T6SS effector, VPA1263 (BAC62606.1), and its cognate immunity protein, Vti2 (WP_005477334.1) [36,37]. Here, we set out to investigate VPaI-6 and similar genomic islands further. We describe a protein trio that defines a widespread mobile genetic element with diverse cargo rich in antibacterial T6SS effectors and anti-phage defense systems. Examining several genes and operons of unknown function within these islands revealed four new anti-phage defense systems. Therefore, the described MGE is akin to a bacterial armory containing diverse offensive and defensive tools against potential rivals, which can be horizontally shared.

Results

GMT proteins define a new class of genomic islands

Analysis of VPaI-6 revealed that the first three genes in this genomic island, encoding VPA1270, VPA1269, and VPA1268 (WP_005477115.1, WP_005477239.1, and WP_005477284.1, respectively), are annotated in the NCBI protein family models database as a Gamma-Mobile-Trio (GMT) system (**Fig. 1a**). We found homologous co-occurring GMT proteins encoded in thousands of Gram-negative and Gram-positive bacterial genomes, including those of pathogenic bacteria, such as *Vibrio*, *Pseudomonas*, *Burkholderia*, *Acinetobacter*, *Enterobacter*, and *Aeromonas* (**Fig. 1b** and **Dataset S1**). Since no information was available on the function of these proteins [35], we set out to investigate the GMT system further.

According to the NCBI Conserved Domain Database [38], the trio's first gene, named *vpa1270* or *gmtY*, encodes a site-specific tyrosine recombinase with a domain belonging to the DNA_BRE_C superfamily. The second gene, *vpa1269*, encodes a phage-like integrase with a domain belonging to the Phage_Integr_2 superfamily, which is predicted to mediate unidirectional site-specific recombination (hereafter, we refer to it as *gmtZ*). The third gene, named *vpa1268* or *gmtX*, encodes a protein of unknown function; we found that it is similar to the DNA binding domain of the partition protein StbA of plasmid R388 (according to HHpred [39], there is 93.44% probability of similarity between amino acids 3-75 of GmtX and amino acids 1-

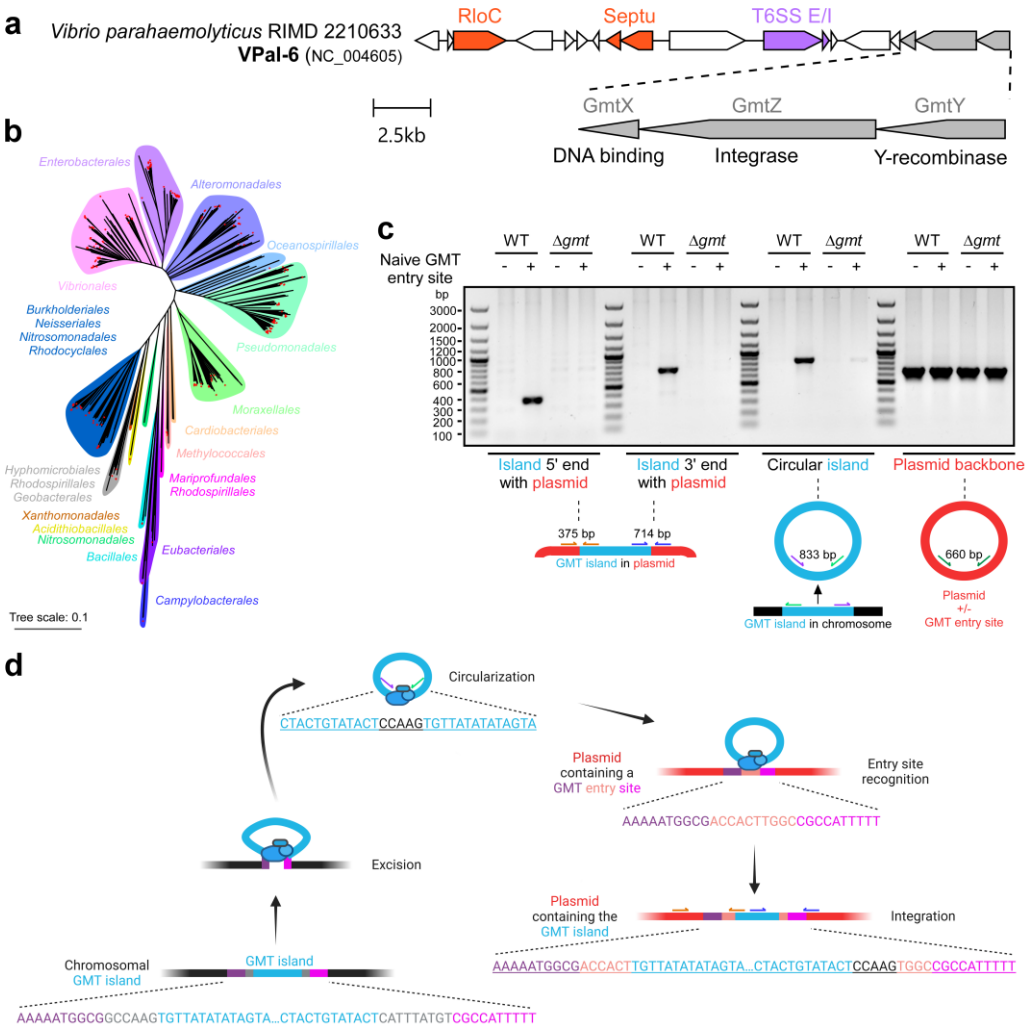

Fig. 1. GMT proteins define a class of widespread, mobile genomic islands. (a) Schematic representation of VPaI-6 and the predicted activities of the GMT protein. **(b)** Phylogenetic distribution of bacteria containing GMT systems, based on the DNA sequence of *rpoB*. Bacterial orders are denoted. The evolutionary history was inferred using the neighbor-joining method. The evolutionary distances represent the number of nucleotide substitutions per site. Red stars denote bacteria in which the borders of a GMT island were determined. **(c)** Agarose gel electrophoresis analysis of the indicated amplicons. The total DNA isolated from wild-type (WT) *V. parahaemolyticus* RIMD 2210633 cells or a derivative in which the GMT system was deleted (Δ*gmt*), conjugated with an empty plasmid or a plasmid containing a predicted 30 bp-long naïve entry site for VPaI-6, was used as a template. Arrows denote the positions of primers used for each amplicon. The *cat* gene found in the backbone of both the empty plasmid and the plasmid containing the naïve entry site was amplified as a control. **(d)** An illustration depicting the mobility of VPaI-6 into a plasmid containing the predicted naïve entry site. Underlined sequences were confirmed by Sanger sequencing the amplicons described in (c). The three dots within cyan-colored sequences denote the GMT island cargo. The three blue blobs denote the GMT system proteins, which may bind the DNA to facilitate excision, entry site recognition, or integration of the island into a naïve entry site.

68 of StbA [PDB: 7PC1_A]). These predicted activities suggest that the GMT system plays a role in DNA mobility.

Systematic analysis of GMT-containing loci (for details, see 'Identification of GMT islands' in the Methods section) revealed that they are found in genomic islands. Comparisons between GMT-containing regions identified in assembled genomes and the genomes of closely related bacteria suggested that GMT-encoding genes define the 5' border of these islands. Sequences flanking the GMT region, which are found adjacent to each other in genomes of closely related bacteria, further revealed the putative 3' border for 83% (366 out of 442) of these GMT islands (**Fig. 1b** and **Dataset S2**). Notably, a genome may contain multiple and diverse GMT islands (e.g., three islands in *Vibrio* sp. B1ASS3), which can reside on the chromosome or a plasmid (**Dataset S1**).

Our analysis also revealed diverse putative entry sites of GMT islands in bacterial genomes, either intragenic or intergenic (**Dataset S2**). When a GMT island appears to have been inserted inside a protein-encoding gene (e.g., *greB*), we often find a homolog of the disrupted gene encoded within the island, possibly to compensate for its loss (**Fig. S1**). In most cases (238 of 366), we identified an inverted repeat as part of the predicted GMT island naïve entry site (**Dataset S2**); the same repeat is often found flanking the GMT island. These observations led us to hypothesize that GMT islands are mobile and that repeat sequences define specific entry sites for each island.

GMT islands are active mobile elements

We posited that if the VPaI-6 GMT island in RIMD is a functional MGE, it should transfer into a naïve entry site. To investigate this possibility, we introduced a plasmid harboring a predicted 30 bp-long naïve, inverted repeat-containing entry site from *V. parahaemolyticus* VP157 (Genbank CP068642.1) into wild-type RIMD cells. Using primer sets designed to amplify fusions between the plasmid sequences flanking the predicted entry site and the 5' or 3' ends of VPaI-6, we found that the RIMD population contains plasmids in which VPaI-6 was inserted into the plasmid (**Fig. 1c**). We confirmed the insertion of VPaI-6 into the specific plasmid-borne entry site with Sanger sequencing of the amplified products (**Fig. 1d** and **File S1**). Furthermore, we revealed the existence of a circular form of the GMT island, lacking the flanking inverted repeats, using primers facing outward from each end of VPaI-6 (**Fig. 1c-d** and **File S1**). The amplification products were missing when we used a RIMD derivative strain in which we deleted the genes encoding the GMT system (Δ*gmt*) or when we modified the spacer sequence between the inverted repeats of the predicted entry site on the plasmid (**Fig. 1c** and **Fig. S2**). Taken together, our results demonstrate that VPaI-6 is a mobile GMT island, which inserts specifically into the repeat-containing site that we identified in the above analyses. The transfer possibly includes an intermediate circular form that excises without the flanking repeat sequences (**Fig. 1d**). Interestingly, isolating a plasmid containing the mobilized VPaI-6 for further analysis posed a challenge, potentially due to the infrequent mobility observed under standard laboratory growth conditions or the possible instability of the resulting plasmid.

GMT islands are rich in defensive and offensive tools

When analyzing the VPaI-6 cargo, we identified a Septu [16] and a RloC [40] anti-phage defense systems (encoded by VPA1260-VPA1261 and VPA1255, respectively) in addition to the previously characterized antibacterial T6SS effector and immunity pair, VPA1263-Vti2 (**Fig. 1a**). The co-occurrence of defense systems and a secreted offensive toxin within the same genomic island was not previously reported, prompting us to investigate whether other GMT islands contain a similarly mixed cargo.

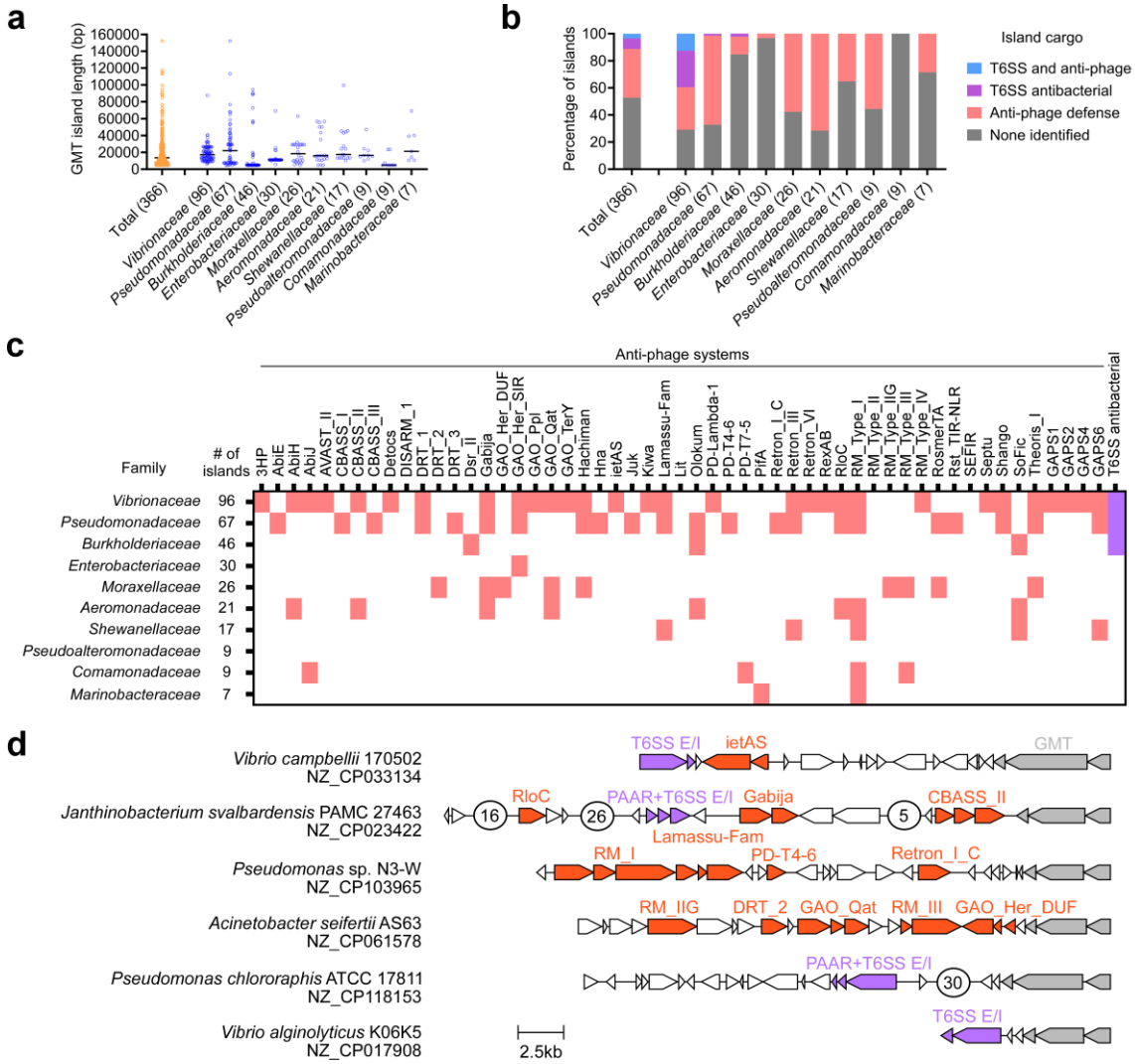

Fig. 2. GMT islands contain diverse cargo of anti-phage defense systems and antibacterial T6SS effectors. (a) Distribution of GMT island lengths, analyzed together (total) of by bacterial family. Black lines denote the median length. **(b)** Percentage of GMT islands in which we identified an anti-phage defense system, an antibacterial T6SS effector, or both together. **(c)** Distribution of specific anti-phage defense systems and antibacterial T6SS effectors in GMT islands of each bacterial family. The analyses in (b-c) include the new anti-phage defense systems identified in this study, as detailed below (i.e., GAPS1, 2, 4, and 6). In (a-c), only bacterial families in which we identified the borders of > 5 GMT islands are shown; the number of analyzed islands is denoted in parenthesis next to the family name. **(d)** The gene structure of representative GMT islands with anti-phage defense systems (red), antibacterial T6SS effectors (purple), or both. Encircled numbers denote the number of genes not shown. RefSeq accession numbers are provided.

We observed considerable variability in the cargo length of the GMT islands for which we identified the borders: between 4.8 and 152.2 kb-long, with a median of ~13.6 kb (**Fig. 2a**). These lengths differ between bacterial families. Notably, some islands are empty, comprising only the genes encoding the GMT system (~ 4.8 kb-long; mainly in *Burkholderiaceae* and *Comamonadaceae* genomes; **Dataset S2**).

Using domains previously associated with secreted T6SS effectors (i.e., VgrG [1], PAAR and PAAR-like [41], MIX [36,37,42,43], FIX [44], and Rhs [45]), we identified antibacterial effectors in ~11% of the examined GMT islands (41 out of 366; **Fig. 2b** and **Dataset S3**). These effectors neighbor a known or predicted immunity gene immediately downstream, and some include a known C-terminal toxic domain (e.g., nuclease or phospholipase). Interestingly, T6SS effectors are prevalent in GMT islands found in members of the *Vibrionaceae* family (~40%; **Fig. 2b** and **Dataset S3**).

Further analysis of GMT island cargoes, using the anti-phage defense system identification servers PADLOC [46] and Defense Finder [47], revealed diverse anti-phage defense systems distributed among most bacterial families (**Fig. 2b-d** and **Dataset S3**). Approximately 40% of the GMT islands contain at least one predicted anti-phage defense system (145 out of 366). Notably, ~12% of the *Vibrionaceae* GMT islands (12 out of 96) contain both anti-phage defense systems and antibacterial T6SS effectors in their cargo (**Fig. 2b,d** and **Dataset S3**). These findings indicate that GMT islands are akin to armories that stockpile defensive and offensive tools against attacking phages and competing bacteria.

GMT islands harbor novel anti-phage defense systems

Many genes within the cargo of GMT islands encode hypothetical proteins with no known function. Since anti-phage defense systems often cluster within so-called 'defense islands' [16,17], we hypothesized that genes of unknown function within GMT islands encode novel anti-phage defense systems. To test this hypothesis, we assembled a list of 13 genes and operons found within GMT islands in members of the genus *Vibrio*, which we predicted are novel anti-phage defense systems; we named them GAPS (GMT-encoded Anti-Phage System) 1 to 13 (**Fig. 3a**).

To investigate their role in defense against phages, we cloned GAPS1-13 into a low-copy number expression plasmid under an arabinose-inducible promoter. *E. coli* K-12 MG1655 ΔRM strains containing the GAPS-encoding plasmids were challenged with 74 coliphages, comprising the 69 coliphages included in the BASEL phage collection [48], T7, T4, $P1_{vir}$, T5, and $lambda_{vir}$. We compared the efficiency of plating (EOP) of the different phages in these strains to *E. coli* harboring a control empty plasmid. Remarkably, four candidates: GAPS1 (WP_005477165.1), GAPS2 (WP_174208646.1), GAPS4 (WP_055466293.1 and WP_055466294.1), and GAPS6 (WP_248387294.1 and WP_248387295.1) provided significant protection against various phages, manifested by a reduction of between two and four orders of magnitude in the number of visible plaques that developed on a lawn of bacteria (i.e., the EOP) (**Fig. 3b**). Six GAPSs (GAPS7, GAPS9, GAPS10, GAPS11, GAPS12, and GAPS13) had no significant protective effect against any of the examined phages. Notably, three candidates were considerably toxic to *E. coli* upon inducible over-expression (GAPS3, GAPS5, and GAPS8); therefore, we could not determine their anti-phage activity. These results support our hypothesis that the cargoes of GMT islands harbor new anti-phage defense systems. Notably, we identified GAPS1, GAPS2, and GAPS6 homologs in several GMT islands, further expanding the list of known anti-phage defense systems encoded within these MGEs (**Fig. 2b-c** and **Dataset S3**)

GAPS1 belongs to the PD-(D/E)xK superfamily of phosphodiesterases

Prompted by these findings, we further investigated one of the newly identified anti-phage systems encoded within VPaI-6, GAPS1, homologs of which are widespread in Gram-negative and Gram-positive bacteria (**Fig. S3** and **Dataset S4**). GAPS1 is a single protein containing a predicted phosphodiesterase domain of the PD-(D/E)xK superfamily [49,50] toward its C-terminus

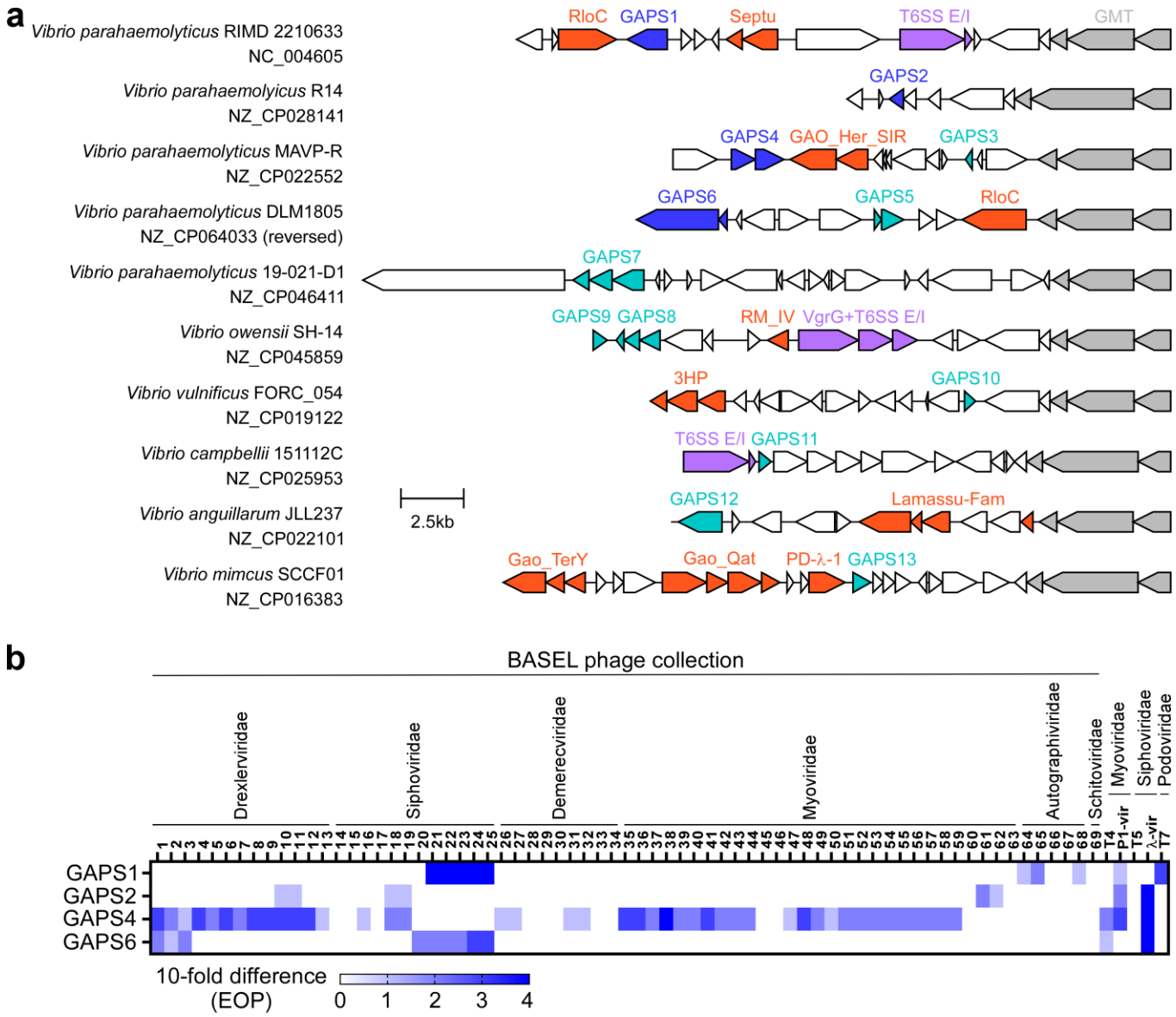

Fig. 3. Four new anti-phage defense systems identified within GMT islands. (a) The gene structure of GMT islands containing GAPS1-13. GAPSs for which anti-phage activity was experimentally confirmed are denoted in blue; other GAPSs are denoted in turquoise. Known anti-phage defense systems (red) and antibacterial T6SS effectors (purple) are also shown. RefSeq accession numbers are provided. **(b)** The efficiency of plating (EOP), indicating the reduction in plaque numbers determined for *E. coli* expressing the four indicted GAPSs when challenged with 74 coliphages, compared to *E. coli* containing an empty plasmid. Coliphage families are denoted above.

(**Fig. 4a**). To determine whether this domain is required for the anti-phage activity of GAPS1, we substituted D313 and K328 within its conserved PD-(D/E)xK active site with alanines. These substitutions abolished the defensive activity against T7 phage, further establishing the role of GAPS1 as an anti-phage defense system and supporting the hypothesis that it uses its phosphodiesterase domain to mediate anti-phage defense (**Fig. 4b**).

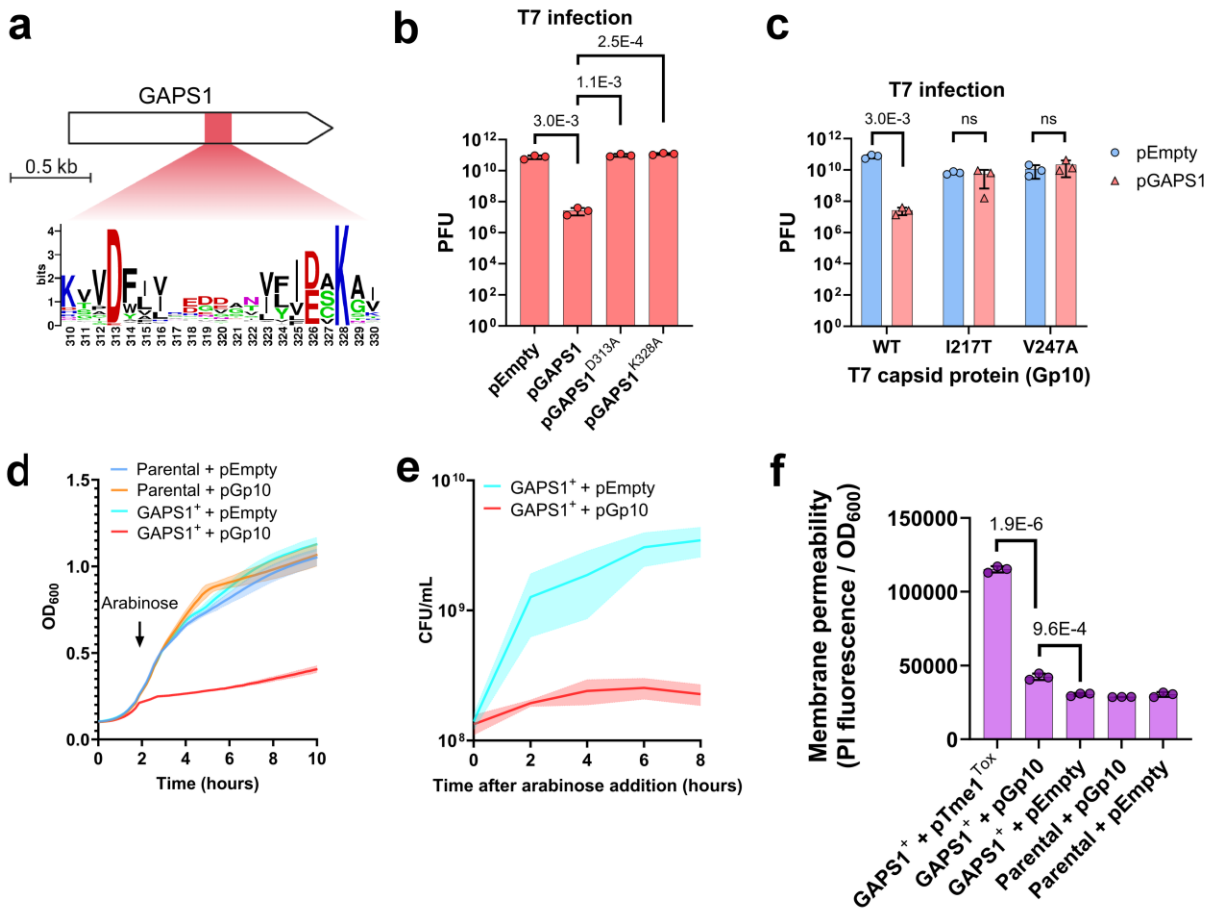

Fig. 4. GAPS1 induces cell dormancy upon activation by a phage capsid protein. (a) Schematic representation of GAPS1 (WP_005477165.1) and the location of the predicted PD-(D/E)xK phosphodiesterase domain. The conservation logo of GAPS1 homologs is shown below. The residue numbers correspond to the positions in WP_005477165.1. **(b)** Plaque forming units (PFU) of T7 phage upon infection of *E. coli* strains containing an empty plasmid (pEmpty) or a plasmid for the arabinose-inducible expression of the indicated GAPS1 version. **(c)** PFU of T7 phage, either wild-type (WT) or containing the indicated mutation in the Gp10 capsid protein, upon infection of *E. coli* strains containing an empty plasmid (pEmpty) or a plasmid for the arabinose-inducible expression of GAPS1 (pGAPS1). **(d)** Growth of *E. coli* strains in which the chromosomal *ydhQ* gene was deleted (Parental) or replaced with an arabinose-inducible GAPS1 ($GAPS1^+$) containing either an empty plasmid (pEmpty) or a plasmid for the arabinose-inducible expression of the T7 phage Gp10 (pGp10). An arrow denotes the time at which arabinose was added. **(e)** Viability (measured as CFU/mL) of $GAPS1^+$ *E. coli* strains containing the indicated plasmids after arabinose addition. **(f)** *E. coli* membrane permeability (measured by the ratio of propidium iodide [PI] fluorescence to OD_{600}) in the indicated strains, 2 hours after arabinose addition to induce protein expression. The C-terminal pore-forming toxic domain of the T6SS effector Tme1 fused to a PelB signal peptide ($pTme1^{Tox}$) was used as a positive control. In (b-f), the data are shown as the mean ± SD of three biological replicates. Statistical significance between samples was determined by an unpaired, two-tailed Student's *t*-test; ns, no significant difference ($P > 0.05$).

A phage capsid protein triggers the anti-phage activity of GAPS1

Next, we sought to identify the phage component that triggers GAPS1. One of the phages against which GAPS1 protects is T7 (**Fig. 3b**). We hypothesized that escape mutants of an attacking T7 phage mutate the protein that triggers GAPS1 to avoid system activation. Therefore, we sequenced the genome of two T7 escape phages that formed plaques in the presence of GAPS1. We identified a mutation in the capsid protein (Gp10)-encoding gene 10 of both isolates; one isolate carried an I217T mutation, and the other a V247A mutation (**Table S1**). Notably, I217 and V247 are spatially close in the folded capsid protein (**Fig. S4**). The escape isolates also contained mutations in other genes; however, these mutations were not common to both isolates.

To determine whether the capsid protein of T7 phage triggers GAPS1-mediated defense, we generated the two mutations identified above in naïve T7 phages. We validated that the additional mutations we identified in the escape isolates are not present in these newly constructed phages, and we tested the ability of GAPS1 to defend against them. We observed no significant difference in the number of mutant T7 phage plaques formed on *E. coli* expressing GAPS1 compared to *E. coli* containing an empty plasmid, indicating that GAPS1 could not defend against the mutant phages (**Fig. 4c**). These findings suggest that the capsid protein is the trigger that activates GAPS1-mediated defense.

GAPS1 induces cell dormancy

Anti-phage defense systems have been proposed to protect bacterial populations by inducing cell suicide, often called abortive infection, or by arresting bacterial growth [51–54]. To determine what mechanism is used by GAPS1, we monitored the effect of its activation on bacterial growth and viability in the absence of T7 phage-derived toxins. Over-expression of the wild-type capsid protein (Gp10) from a plasmid inhibited the growth of *E. coli* expressing a chromosomally inserted GAPS1 (**Fig. 4d**). These arrested cells were protected from ampicillin-induced lethality, indicating that they were not actively dividing or synthesizing peptidoglycan [55] (**Fig. S5**). Importantly, we did not observe a reduction in cell viability over time (**Fig. 4e**) or a substantial increase in membrane permeability (**Fig. 4f**), demonstrating that Gp10-triggered GAPS1 activity is not bactericidal. These results suggest that GAPS1 is a member of the PD-(D/E)xK phosphodiesterase superfamily that induces cell dormancy rather than cell suicide upon recognizing a phage capsid protein.

E. coli GAPS1 homologs are bona fide anti-phage defense systems

The results demonstrating anti-phage defense against coliphages were obtained by over-expressing an exogenous GAPS1 originating from *V. parahaemolyticus* in *E. coli*. To confirm that endogenous *E. coli* GAPS1 protects against coliphages, we cloned three *E. coli* GAPS1 homologs, EGQ2075554.1, EJP5250929.1, and WP_152927281.1, into the same low-copy number expression plasmid used to investigate the *Vibrio* GAPS candidates; these homologs share 24-29% amino acid identity with GAPS1 across 64-96% of its length (**Fig. S6**). As predicted, these three GAPS1 homologs protected *E. coli* against diverse coliphages in our array (**Fig. 5a**).

Importantly, we also obtained a clinical *E. coli* isolate, ZH142-A (isolated from a human rectal swab; BioSample: SAMN13943461), naturally encoding a GAPS1 homolog (WP_194242909.1; **Fig. S6**). Remarkably, the *E. coli* ZH142-A GAPS1 homolog was required to protect this strain against BASEL collection phage 21 (**Fig. 5b**; BASEL21). While the growth of the wild-type strain was largely unaffected when challenged with a low phage multiplicity of infection (MOI 0.5), a high MOI (5) led to growth arrest, as we observed for *E. coli* exogenously expressing the *Vibrio* GAPS1 together with its T7 phage trigger, Gp10 (**Fig. 4d**). However, in the absence of the

endogenous GAPS1 (Δ*gaps1*), cell lysis was evident when ZH142-A bacteria were challenged with a high phage MOI (**Fig. 5c**). Taken together, these results confirm that GAPS1 establishes a novel family of anti-phage defense systems.

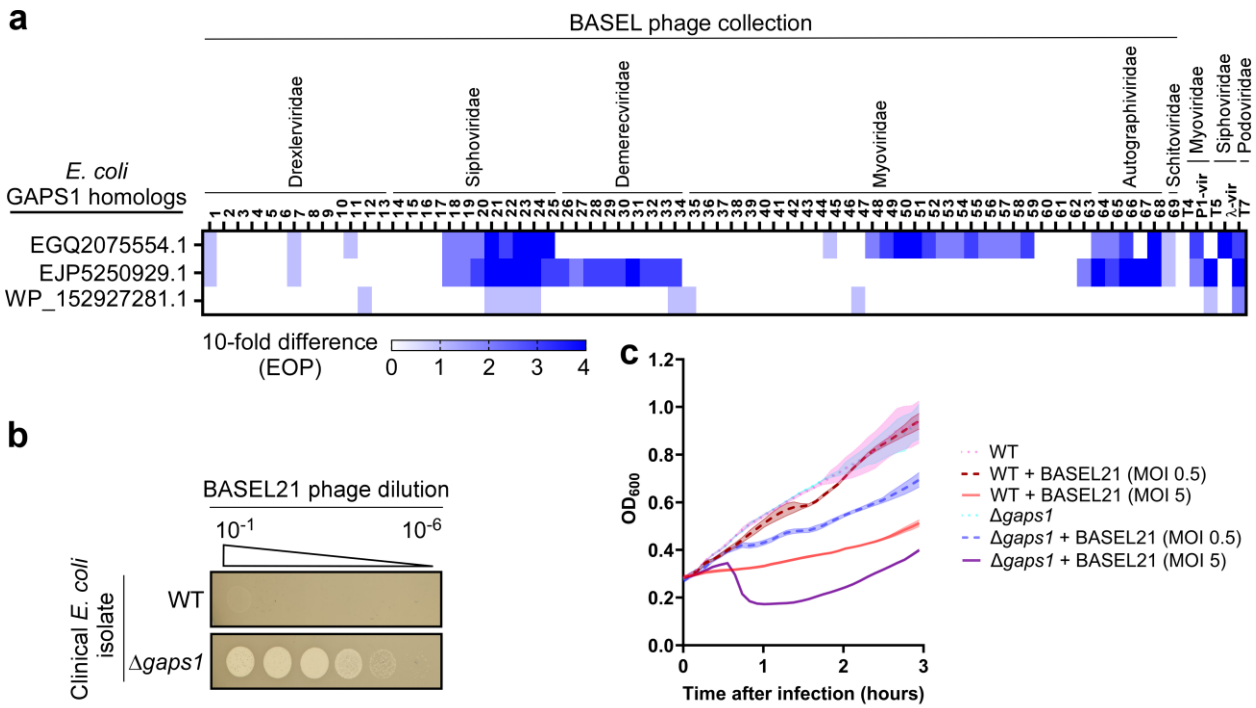

Fig. 5. *E. coli* GAPS1 homologs protect against various coliphages. (a) The efficiency of plating (EOP) determined for *E. coli* expressing the three indicted GAPS1 homologs when challenged with 74 coliphages, compared to *E. coli* containing an empty plasmid. **(b)** Tenfold serial dilutions of the BASEL collection phage 21 (BASEL21) spotted on lawns of *E. coli* isolate ZH142-A, either wild-type (WT) or with a deletion of it endogenous GAPS1 homolog (Δ*gaps1*). **(c)** Growth of the indicated *E. coli* ZH142-A cells following infection with the BASEL21 phage at MOI of 0.5 or 5. Data are shown as the mean ± SD of three biological replicates.

Discussion

An evolutionary arms race forces bacteria to acquire new offensive and defensive tools to outcompete rival bacteria and survive phage attacks. Although HGT plays a significant role in this arms race [56], many mechanisms that mediate HGT in bacteria are poorly understood. Here, we describe GMT, a new system akin to a mobile armory that equips bacteria with defensive and offensive tools.

Anti-phage defense systems have been found in the cargo of MGEs [13,20,28,29] and shown to often cluster in so-called 'defense islands'. They have also been reported to neighbor other defensive tools, such as antibiotic resistance genes, within MGEs [57,58]. Secreted antibacterial toxins were also identified within MGEs [31–33,59]. However, GMT islands are the first example of an MGE carrying such defensive and offensive tools together or interchangeably. Although predominantly prevalent in *Vibrionaceae* GMT islands, this phenomenon may be common. MGEs previously regarded strictly as 'defense islands' should be re-analyzed, considering they might contain new antibacterial offensive tools. Moreover, since bacteria use GMT islands to acquire anti-phage defense systems and antibacterial toxins interchangeably, these defensive

and offensive tools possibly fall under the same category. Therefore, we propose that secreted antibacterial toxins be considered a bacterial immune mechanism, equivalent to anti-phage defense systems.

We propose plasmids could be a mechanism for disseminating GMT islands via HGT. In support of this notion, we find many examples of GMT islands on plasmids (**Dataset S1**). Some bacteria even contain two identical GMT islands, one on the chromosome and another on a plasmid (**Dataset S2**). In *V. alginolyticus*, for example, the predicted chromosomal and plasmid naïve entry sites share inverted repeat sequences with an identical 5' AAGAGC 3' core separated by a 14 bp-long spacer (**Fig. S7**). Therefore, it is possible that if a naïve entry site is found on a plasmid, a GMT island can transfer from the chromosome to the plasmid and then exploit the plasmid to reach other bacteria via HGT.

Many genes within the cargo of GMT islands have no known function. We leveraged the finding that these MGEs are rich in defensive tools to reveal four new anti-phage defense systems. Notably, the investigated GAPSs originate from vibrios, yet we examined them in *E. coli* as a surrogate platform against a set of coliphages. Furthermore, we showed that an endogenous GAPS1 homolog in *E. coli* protects it against a native coliphage. Although we could not confirm their role against phages, the nine GAPSs that did not protect against coliphages may defend against a *Vibrio*-specific phage when expressed in their natural host. Alternatively, additional regulatory or accessory components endogenously found in vibrios might be required for defense activity. In light of our findings, we predict that many other genes within GMT islands encode novel anti-phage defense systems or even novel, secreted antibacterial toxins.

GAPS1, encoded on VPaI-6, represents a new widespread family of anti-phage defense systems. Being a single protein, GAPS1 probably contains both the sensor that recognizes the phage trigger (i.e., a capsid protein) and the effector, which we predict is its PD-(D/E)xK phosphodiesterase domain. By identifying the phage trigger, we could decipher the outcome of GAPS1 activation being cell dormancy rather than cell death. However, since the target of GAPS1 activity remains unknown, it is unclear whether GAPS1 merely inhibits cell growth to halt the progression of the phage infection cycle. It is possible that GAPS1 also actively eliminates the invading phage threat, thus allowing for cell recovery.

Although widespread, the GMT system is predominantly found in gamma-proteobacteria, some beta-proteobacteria, and a handful of Gram-positive families. Nevertheless, our analysis of GMT homologs in this work was conservative, considering only systems highly similar to the trio found in VPaI-6. More distant trios may exist in other bacterial families, and their cargo could contain additional defensive and offensive tools. In future work, we will determine whether GMT systems are regulated, and what is the role of GMT components in the mobility mechanism. We will also decipher how each system identifies a unique and specific entry site. Further investigation of these intriguing mobile armories will shed light on bacterial interactions, evolution, and HGT.

Methods

Strains and media: For a complete list of strains used in this study, see **Table S2**. *Escherichia coli* strains were grown in Lysogeny Broth (LB; 1% [wt/vol] tryptone, 0.5% [wt/vol] yeast extract, and 0.5% [wt/vol] NaCl) or 2xYT (1.6% [wt/vol] tryptone, 1% [wt/vol] yeast extract, and 0.5% [wt/vol] NaCl) at 37°C. *Vibrio parahaemolyticus* strains were grown in Marine Lysogeny Broth (MLB; LB containing 3% [wt/vol] NaCl) and on Marine Minimal Media (MMM) agar plates (1.5% [wt/vol] agar, 2% [wt/vol] NaCl, 0.4% [wt/vol] galactose, 5 mM $MgSO_4$, 7 mM K_2SO_4, 77 mM

K_2HPO_4, 35 mM KH_2PO_4, and 2 mM NH_4Cl) at 30°C. Media were supplemented with 1.5% (wt/vol) agar to prepare solid plates. When required, media were supplemented with 35 or 10 µg/mL chloramphenicol (for *E. coli* and V*. parahaemolyticus*, respectively), 50 or 250 µg/mL kanamycin (for *E. coli* and V*. parahaemolyticus*, respectively), or 100 µg/mL ampicillin to maintain plasmids. To induce the expression from Pbad promoters, 0.04% or 0.2% (wt/vol) L-arabinose was added to the media, as indicated.

Plasmid construction: Plasmids were constructed with standard molecular biology techniques using the Gibson Assembly method [60]. The Gibson Assembly master mix was obtained from NEB (E2611S). DNA fragments were amplified by PCR from bacterial genomic DNA or from DNA synthesized by TWIST Bioscience, and Gibson Assembly ligations were carried out according to the manufacturer's instructions. Commercially synthesized DNA, plasmids, and primers that were used in this study are listed in **Table S3**, **Table S4**, and **Table S5**, respectively.

Generating *Vibrio parahaemolyticus* mutant strains: For in-frame deletion of the genes vpa1270-vpa1268 encoding GmtY, GmtZ, and GmtX in *V. parahaemolyticus* RIMD 2210633, 600 bp-long sequences upstream and downstream of this region were cloned into pDM4, a Cm^R OriR6K suicide plasmid [61]. Next, the pDM4 constructs were transformed into *E. coli* DH5α (λ pir) by electroporation, and then conjugated into *V. parahaemolyticus*. Trans-conjugants were selected on MMM agar plates containing chloramphenicol. The resulting trans-conjugants were grown on MMM agar plates containing 15% [wt/vol] sucrose for counter-selection and loss of the SacB-containing pDM4. Deletions were confirmed by PCR.

VPaI-6 mobility assays: pBAD33.1 plasmids, either empty or containing a 30 bp-long predicted VPaI-6 entry site from *V. parahaemolyticus* VP157 or its mutated form in its multiple cloning site (**Fig. S2b**), were transformed into *E. coli* Neb5α and subsequently introduced into *V. parahaemolyticus* RIMD 2210633 or its Δ*gmt* mutant via tri-parental mating. The resulting conjugated colonies were selectively grown on MMM agar plates supplemented with 10 µg/mL chloramphenicol. Then, all the colonies that grew on the selective plates were harvested, resuspended in LB media, and subjected to total genomic DNA isolation using the PrestoTM Mini gDNA isolation kit.

To identify instances in which VPaI-6 mobilized from the chromosome into the pBAD33.1-based plasmid, we used the abovementioned total DNA isolations as template and performed PCR using primer sets intended to amplify: (i) a fusion between the plasmid and the 5' end of VPaI-6, (ii) a fusion between the plasmid and the 3' end of VPaI-6, (iii) a fusion between the 5' and 3' ends of VPaI-6 (i.e., circularization), and (iv) a Cm^R gene (within the pBAD33.1 backbone; used as an internal control for plasmid presence). The PCR products were resolved using a 1% agarose gel and visualized using EtBr.

Plaque assays: The phages used in this study are listed in **Table S6**. Phages were propagated on *E. coli* K12 MG1655 ΔRM. To determine the effect of the 13 putative defense system (GAPS1-13) against coliphages T4, T5, T7, $lambda_{vir}$, $P1_{vir}$, and the 69 phages included in the BASEL collection [48], *E. coli* K12 MG1655 ΔRM strains harboring the indicated pBAD33.1-based plasmids were grown overnight in LB supplemented with chloramphenicol and 0.2% (wt/vol) D-glucose (to repress expression from the pBAD promoter) at 37°C. Overnight cultures were washed twice to remove any remaining glucose, and then 350 µL of each culture were mixed with 7 mL of 0.7% (wt/vol) molten agar supplemented with 0.2% (wt/vol) L-arabinose, 10 mM $MgSO_4$, and 5 mM $CaCl_2$. The mixture was poured onto a 1.5% (wt/vol) agar plate supplemented with chloramphenicol and 0.2% (wt/vol) L-arabinose, and the plates were left to dry. Tenfold serial dilutions of all the phages were prepared, and 7.5 µL of each dilution were spotted on the dried plates. The plates were incubated overnight at 37°C. The following day, the

plaques were counted and the plaque forming units (PFU/mL) were calculated. For dilution spots in which no individual plaques were visible but a faint zone of lysis was observed, the dilution was considered as having ten plaques, as previously described [62]. Plaque assays with *E. coli K12* MG1655 ΔRM containing plasmids for the expression of GAPS1 mutants and homologs were performed similarly. This protocol was also used to investigate the ability of BASEL collection phage 21 to form plaques on *E. coli* ZH142-A and its Δ*gaps1* mutant, except the plates did not include L-arabinose or antibiotics.

Isolation of T7 escape phages: *E. coli* BW25113 harboring an empty pBAD33.1 or one encoding GAPS1 (pBAD33.1-GAPS1) was grown overnight in LB supplemented with chloramphenicol and 0.2% (wt/vol) D-glucose at 37°C. The cells were washed twice and mixed with 0.7% (wt/vol) molten agar supplemented with 0.2% (wt/vol) L-arabinose, and poured onto a 1.5% (wt/vol) agar plate supplemented with 0.2% (wt/vol) L-arabinose. After the agar dried, 10-fold serial dilutions of a T7 phage suspension were spotted onto the plate, and the plate was incubated overnight at 37°C. Individual plaques growing at the highest dilution on the plates containing *E. coli* expressing GAPS1 were isolated and propagated on naïve *E. coli* BW25113 cells harboring pBAD33.1-GAPS1 in LB supplemented with chloramphenicol and 0.2% (wt/vol) L-arabinose at 37°C. The escape phages were confirmed by spotting them on plates with *E. coli* expressing GAPS1.
For phage genomic DNA isolation, high titers of escape phages and a parental wild-type phage were prepared (~$1.0E^{11}$ PFU/mL). Approximately 40 mL of lysates of each escape phage were mixed with 10% (wt/vol) PEG 8000 and 3 M NaCl, and incubated overnight at 4°C. The lysate-PEG mixture was then centrifuged at 10000 x *g* for 15 minutes to collect the phage pellet. The pellet was re-suspended using resuspension buffer from the Presto™ Mini gDNA isolation kit, and the phage genomic DNA was isolated following the manufacturer's protocol.

Illumina whole-genome sequencing was carried out at SeqCenter (Pittsburgh, PA, USA; https://www.seqcenter.com/). Sample libraries were prepared using the Illumina DNA Prep kit and IDT 10 bp UDI indices, and sequenced on an Illumina NextSeq 2000, producing 2 x 151 bp reads. Mutations were identified using variant calling (SeqCenter). Only mutations that were found in the escape mutant genomes and that were not in the sequenced parental T7 phage are reported in **Table S1**.

Constructing T7 phage mutants: T7 mutants were constructed using the pORTPHAGE method [63], a MAGE [64,65]-based system for the mutagenesis of bacteriophages. Briefly, *E. coli* K-12 strain harboring the pORTMAGE-Ec1 plasmid was grown to reach early log phase (OD_{600} ~0.3). Then, 1 mM m-toluic acid was added to induce the expression of recombineering proteins. The cells were made electrocompetent, and then transformed with mutating oligonucleotides. After electroporation, the culture was infected with a wild-type T7 phage and incubated until complete lysis occurred. The final lysate was cleared using chloroform, diluted, and then plated using the soft agar overlay method to screen for individual mutated plaques. Single plaques were picked, suspended in LB, and used as templates for PCR amplification and sequencing to identify mutants.

Chromosomal integration of GAPS1: GAPS1 was introduced into the chromosome of *E. coli* BW25113 in place of *ydhQ* (*ydhQ*::GAPS1) using the red recombination system, as previously described [66]. Briefly, *E. coli* BW25113 cells harboring pSim6 were grown overnight in LB supplemented with ampicillin at 30°C. Overnight cultures were diluted 1:100 in 35 mL of fresh LB supplemented with ampicillin, and grown to an OD_{600} of ~0.5. The red recombinase system was then heat-induced for 20 minutes in a shaking water bath at 42°C. Immediately after induction, the cells were chilled on ice and pelleted by centrifugation. The cell pellets were washed thrice with ice-cold water and resuspended in 200 µL of ice-cold water. The gene encoding GAPS1 under P_{BAD} promoter control, along with a kanamycin-resistance cassette, was

amplified together with flanking sequences identical to flanking sequences 50 bp upstream and downstream of the chromosomal *ydhQ*. The amplified DNA was treated with DpnI, and then run on an agarose gel and purified. The purified DNA was electroporated into *E. coli*, and bacteria were allowed to recover in 2xYT broth supplemented with 0.2% (wt/vol) D-glucose for 2 hours at 30°C. The transformed cells were then plated onto a 1.5% (wt/vol) agar plate supplemented with 25 µg/mL kanamycin. The integration of GAPS1 was verified by PCR. Bacteria were cured of the pSIM6 plasmid, and the recombinant cells were electroporated with pCP20 plasmid. The kanamycin cassette was flipped out by inducing the pCP20 plasmid at 42°C.

Deleting the GAPS1 homolog in *E. coli* ZH142-A: The GAPS1 homolog was deleted from the chromosome of *E. coli* ZH142-A using the lambda red recombination system, and replaced with a kanamycin resistance cassette. A single colony of bacteria containing the pSim6 plasmid was grown overnight in LB supplemented with ampicillin at 30°C. The overnight culture was diluted 1:100 in 35 mL of fresh LB supplemented with ampicillin and grown to an OD_{600} of ~0.5. The red recombinase system was then heat-induced for 20 minutes in a shaking water bath at 42°C. Immediately after induction, the cells were chilled on ice and pelleted by centrifugation. The cell pellets were washed thrice with ice-cold water and resuspended in 200 µL of ice-cold water. Then, these cells were electroporated with the following DNA: The kanamycin-resistance cassette, along with the flippase recognition target (FRT) sites, was amplified from *E. coli* BW25113ΔydhQ::kan using primer pairs with overhang sequences homologous to the 50 bp of the 5' and 3' sequences flanking the GAPS1 homolog. The amplified DNA was treated with DpnI restriction enzyme, run on an agarose gel, and purified.

Following electroporation, the cells were allowed to recover in 2xYT broth for 2 hours at 30°C. The transformed cells were then plated onto a 1.5% (wt/vol) agar plate supplemented with 25 µg/mL kanamycin. The replacement of the GAPS1 homolog with the kanamycin resistance cassette was verified by PCR. Bacteria were subsequently cured of the pSIM6 plasmid [67].

***E. coli* toxicity and viability assays:** *E. coli* BW25133 Δ*ydhQ* and *E. coli* BW25133 *ydhQ*::GAPS1 cells harboring an empty plasmid or a plasmid for the arabinose-inducible expression of the T7 phage gene10 (encoding the Gp10 capsid protein) were grown overnight at 37°C in LB supplemented with kanamycin and 0.2% (wt/vol) D-glucose. Overnight cultures were diluted to an OD_{600} = 0.02 in fresh LB supplemented with kanamycin, and 200 µL were transferred into 96-well plates in triplicate. Cells were grown under continuous shaking (205 RPM) in a Tecan Infinite M Plex plate reader at 37°C. After 2 hours, the expression of Gp10 and GAPS1 was induced by adding L-arabinose to a final concentration of 0.2% (wt/vol). OD_{600} readings were acquired every 10 minutes. A similar procedure was used to determine the effect of adding ampicillin (100 µg/mL) 1 hour after arabinose addition.

To determine cell viability after induction, bacteria were collected at the indicated time points after arabinose addition. Tenfold serial dilutions of each culture were spotted on 1.5% (wt/vol) agar plates supplemented with kanamycin and 0.2% (wt/vol) D-glucose (to repress arabinose-induced expression). The plates were incubated overnight at 37°C, and the CFU/mL of each culture were determined the following day.

To monitor membrane permeability, *E. coli* BW25113 *ydhQ*::GAPS1 strains containing the indicated plasmids were grown overnight at 37°C in 2xYT supplemented with kanamycin and 0.2% (wt/vol) D-glucose. Overnight cultures were washed twice and diluted 1:100 in fresh 2xYT supplemented with kanamycin and grown for 2 hours at 37°C. Then, L-arabinose was added to the media (final concentration of 0.1% [wt/vol]) to induce expression from Pbad promoters. Cells were grown for 2 additional hours and then normalized to OD_{600} of 0.5. Cells were washed twice with 1 mL of filter-sterilized 1xPBS, and 200 µL were transferred in triplicate into a black, flat-bottom 96-well plate (Greiner). Then, 10 µL of propidium iodide (PI; Sigma) were added to each

well, resulting in a final PI concentration of 1 µg/mL. Following a 15-minute incubation in the dark at room temperature, OD_{600} and PI fluorescence were determined using a Tecan Infinite M Plex microplate reader. PI fluorescence was detected using excitation at 540 nm and emission at 621 nm. The C-terminal toxic domain of the pore-forming Tme1 T6SS effector fused to an N-terminal PelB signal peptide [68] was used as a positive control.

To monitor bacterial growth upon infection with BASEL collection phage 21, *E. coli* ZH142-A wild-type and Δ*gaps1* mutant strains were grown overnight at 37°C in LB. Overnight cultures were diluted 1:100 in 10 mL of fresh LB and grown to an OD_{600} of ~0.3. The phage was then added to the bacterial cultures at the indicated MOI, and 200 µL of cells were transferred into 96-well plates in triplicate. Cells were grown under continuous shaking (205 RPM) in a Tecan Infinite M Plex plate reader at 37°C. OD_{600} readings were acquired every 10 minutes.

Identification of GMT islands: GMT islands were identified by performing the following steps.

Construction of position-specific scoring matrices (PSSMs) of GMT proteins.

The PSSMs of VPA1270 (GmtY), VPA1269 (GmtZ), and VPA1268 (GmtX) were constructed using full-length sequences from *Vibrio parahaemolyticus* RIMD 2210633 (WP_005477115.1, WP_005477239.1, and WP_005477284.1, respectively). To improve the identification of GMT proteins, additional PSSMs of VPA1269 and VPA1268 were constructed using full-length sequences from *Vibrio parahaemolyticus* R14 (WP_108745444.1 and WP_085344822.1, respectively). In each case, five iterations of PSI-BLAST against the RefSeq protein database were performed. A maximum of 500 hits with an expect value threshold of 10^{-6} and a query coverage of 70% were used in each iteration of PSI-BLAST.

Identification of bacterial genomes containing GMT systems.

A local database containing the RefSeq bacterial nucleotide and protein sequences was generated (last updated on August 21, 2023). RPS-BLAST was used to identify GmtY homologs in the local database. The results were filtered using an expect value threshold of 10^{-6} and a query coverage of 70%. Analysis was limited to complete genomes (NCBI assembly level: complete genome or chromosome). Subsequently, the genomic neighborhood of GmtY-containing genomes was analyzed as described before [43,69,70]. The results were further analyzed to identify bacterial sequences containing the three GMT proteins in tandem. Cases where an unrelated protein was inserted between GMT proteins (*e.g.*, a transposase) were accommodated. A list of GMT proteins and adjacently encoded proteins is provided in **Dataset S1.**

Identification of closely related genomes.

First, the sequences of *rpoB*, coding for DNA-directed RNA polymerase subunit beta, were retrieved from the local database for all RefSeq bacterial genomes. Partial and pseudo-gene sequences were excluded. A nucleotide database of *rpoB* genes was generated. Next, BLASTN was performed using the sequences of *rpoB* from the GMT-containing genomes as queries to identify *rpoB* homologs with high sequence identity (at least 90% over at least 90% of the sequence). The BLASTN results were analyzed and a list of closely related genomes was generated for each GMT-containing genome.

Identification of genomic accessions in closely related genomes that are homologous to sequences flanking GMT systems.

The nucleotide sequences of the GMT systems and their 5' and 3' flanking regions, up to 200 kbp of either side of *GmtY*, were retrieved. These sequences were used as query in BLASTN against the nucleotide sequences of closely related genomes. The results were filtered to include local alignments that are of ≥1 kbp length with ≥80% identity between aligned

sequences. The alignments were further analyzed to identify separate alignments belonging to the same genomic accessions that flank the GMT systems but do not include them (**Fig. S8a**). The alignments were required to be with the same strand of the subject accession. The distances between the positions of the alignments in the subject accessions were required to be ≤100 bp (**Fig. S8a**). In addition to the above criteria, the sequences upstream and downstream to the GMT islands were required to contain sequence alignments to the subject accessions in at least 4 kbp out of 10 kbp upstream and downstream sequences. The aim of this step was to remove false alignments due to frequent sequences (e.g., transposases) (**Fig. S8b**).

Identification of GMT Island borders.

The alignments meeting all the abovementioned requirements were grouped together to determine the 5' and 3' borders of GMT islands (**Figure S8c**). First, the consensus values of the borders were deduced based on the most frequently occurring values. Then, the putative borders were ranked based on the following criteria: (i) distance between subject alignments ≤20 bp, (ii) upstream and downstream alignments ≥5 kbp, (iii) borders are ±10 bp from consensus values, and (iv) borders are exactly the same as the consensus values. The putative borders with the highest ranking were selected for further analysis (**Dataset S2**).

Analysis of the putative entry sites.

The predicted entry site for each GMT island was determined according to positions of the alignments in the subject accessions. Entry sites were defined as 'intragenic' or 'intergenic' if located inside or outside genes, respectively (**Fig. S8d**). The sequences located 25 bp from the ends of the predicted entry sites were analyzed to identify direct and inverted repeats (**Fig. S8e**). Briefly, to identify direct repeats, all possible sub-sequences located in the first sequence were searched in the second sequence. To identify inverted repeats, the search was performed in the reverse complement. The minimal repeat size was set to 5 nucleotides, and the longest identified repeats were saved.

Analysis of GMT island cargoes: T6SS effectors were identified by the presence of T6SS effector-specific domains (i.e., MIX [36,43], FIX [44], Rhs [45], PAAR and PAAR-like [41], Hcp [1], and VgrG [1]), determined by NCBI Conserved Domain Database (CDD) [38] (see below) or using previously-constructed PSSMs. Predicted toxic domains of T6SS effectors were identified using CDD or by similarity detection using hidden Markov modeling (HHpred [71]). Small genes downstream of T6SS effectors were annotated as putative immunity genes. Anti-phage defense systems were identified using the PADLOC [46] and DefenseFinder [47] tools. In the case of PADLOC, amino acid sequences and gff3 files of the complete genomes were provided as input. In the case of DefenseFinder, amino acids sequences, ordered according to their position in the genomes, were provided as input. The anti-phage defense systems described in this work were identified by constructing PSSMs for proteins belonging to the systems and identification of homologs using RPS-BLAST. PSSMs of GAPS1, GAPS4a, GAPS4b, GAPS6a, and GAPS6b were constructed using full-length sequences (WP_005477165.1, WP_055466293.1, WP_055466294.1, WP_248387294.1, and WP_248387295.1, respectively). PSI-BLAST was performed as described above for the GMT system. RPS-BLAST results were filtered using an expect value threshold of 10^{-15} and a minimal coverage of 70%. With regard to GAPS4 and GAPS6, all proteins belonging to these systems were required for the systems to be counted.

Identification of conserved domains: The CDD and related information were downloaded from NCBI on August 27, 2023 [38]. RPS-BLAST was employed to identify conserved domains in protein sequences and the output was processed using the Post-RPS-BLAST Processing Utility v0.1. The expect value threshold was set to 10^{-5}.

Construction of phylogenetic trees: Phylogenetic analysis of bacterial strains was conducted using the MAFFT server (mafft.cbrc.jp/alignment/server/) [72]. The nucleotide sequences of *rpoB* were aligned using MAFFT version 7 (FFT-NS-i) [73]. Partial and pseudo-gene sequences were not included in the analysis. The evolutionary history was inferred using the neighbor-joining method [74] with the Jukes-Cantor substitution model (JC69). The indicated evolutionary distances are in the units of the number of base substitutions per site.

Illustration of conserved residues using Weblogo: The protein sequences of GAPS1 homologs were aligned using CLUSTAL Omega [75]. Aligned columns not found in representative proteins were discarded. The conserved residues were illustrated using the WebLogo server (weblogo.berkeley.edu) [76].

Multiple sequence alignment of *E. coli* GAPS1 homologs: The amino acid sequences of EGQ2075554.1, EJP5250929.1, WP_152927281.1, WP_194242909.1, and GAPS1 (WP_005477165.1) were aligned using Clustal W [77] in MEGA X [78]. Similarity and identity shading was done in ESPript 3.0 [79].

Acknowledgments

We thank members of the Salomon, Qimron, and Bosis laboratories for helpful discussions and suggestions. We also thank Andrea Endimiani (University of Bern) for gifting us the *E. coli* ZH1420A strain, and Alexander Harms (ETH Zurich) for generously sharing the BASEL phage collection. DS and EB received funding from the Israel Science Foundation (ISF grant number 1362/21). UQ is supported by the European Research Council – Horizon 2020 research and innovation program, grant no. 818878. UQ has also received funding from the Israeli Ministry of Health in the framework of the ERANET-JPI-AMR, grant no. 15370. KK was supported by a PhD Scholarship from the Tel Aviv University Center for Combatting Pandemics. Several figures were prepared using biorender.com.

References

1. Pukatzki, S. *et al.* Identification of a conserved bacterial protein secretion system in Vibrio cholerae using the Dictyostelium host model system. *Proc. Natl. Acad. Sci.* **103**, 1528–1533 (2006).
2. Hood, R. D. *et al.* A type VI secretion system of Pseudomonas aeruginosa targets a toxin to bacteria. *Cell Host Microbe* **7**, 25–37 (2010).
3. Jana, B. & Salomon, D. Type VI secretion system: a modular toolkit for bacterial dominance. *Future Microbiol.* **14**, fmb-2019-0194 (2019).
4. MacIntyre, D. L., Miyata, S. T., Kitaoka, M. & Pukatzki, S. The Vibrio cholerae type VI secretion system displays antimicrobial properties. *Proc. Natl. Acad. Sci.* **107**, 19520–19524 (2010).
5. Allsopp, L. P. & Bernal, P. Killing in the name of: T6SS structure and effector diversity. *Microbiology* **169**, 001367 (2023).
6. Speare, L. *et al.* Bacterial symbionts use a type VI secretion system to eliminate competitors in their natural host. *Proc. Natl. Acad. Sci. U. S. A.* **115**, E8528–E8537

(2018).

7. Ma, L. S., Hachani, A., Lin, J. S., Filloux, A. & Lai, E. M. Agrobacterium tumefaciens deploys a superfamily of type VI secretion DNase effectors as weapons for interbacterial competition in planta. *Cell Host Microbe* **16**, 94–104 (2014).

8. Borgeaud, S., Metzger, L. C., Scrignari, T. & Blokesch, M. The type VI secretion system of Vibrio cholerae fosters horizontal gene transfer. *Science* **347**, 63–7 (2015).

9. Sana, T. G. *et al. Salmonella* Typhimurium utilizes a T6SS-mediated antibacterial weapon to establish in the host gut. *Proc. Natl. Acad. Sci.* **113**, E5044–E5051 (2016).

10. Verster, A. J. *et al.* The Landscape of Type VI Secretion across Human Gut Microbiomes Reveals Its Role in Community Composition. *Cell Host Microbe* **22**, 411-419.e4 (2017).

11. Unterweger, D. *et al.* The Vibrio cholerae type VI secretion system employs diverse effector modules for intraspecific competition. *Nat. Commun.* **5**, 3549 (2014).

12. Pleška, M., Lang, M., Refardt, D., Levin, B. R. & Guet, C. C. Phage-host population dynamics promotes prophage acquisition in bacteria with innate immunity. *Nat. Ecol. Evol.* **2**, (2018).

13. Hussain, F. A. *et al.* Rapid evolutionary turnover of mobile genetic elements drives bacterial resistance to phages. *Science (80-.).* **374**, 488–492 (2021).

14. Piel, D. *et al.* Phage–host coevolution in natural populations. *Nat. Microbiol. 2022 77* **7**, 1075–1086 (2022).

15. Hampton, H. G., Watson, B. N. J. & Fineran, P. C. The arms race between bacteria and their phage foes. *Nature* vol. 577 (2020).

16. Doron, S. *et al.* Systematic discovery of antiphage defense systems in the microbial pangenome. *Science* **359**, eaar4120 (2018).

17. Makarova, K. S., Wolf, Y. I., Snir, S. & Koonin, E. V. Defense Islands in Bacterial and Archaeal Genomes and Prediction of Novel Defense Systems. *J. Bacteriol.* **193**, (2011).

18. Bernheim, A. & Sorek, R. The pan-immune system of bacteria: antiviral defence as a community resource. *Nat. Rev. Microbiol. 2019 182* **18**, 113–119 (2019).

19. Millman, A. *et al.* An expanded arsenal of immune systems that protect bacteria from phages. *Cell Host Microbe* **30**, 1556-1569.e5 (2022).

20. Vassallo, C. N., Doering, C. R., Littlehale, M. L., Teodoro, G. I. C. & Laub, M. T. A functional selection reveals previously undetected anti-phage defence systems in the E. coli pangenome. *Nat. Microbiol. 2022 710* **7**, 1568–1579 (2022).

21. Le Roux, F. & Blokesch, M. Eco-evolutionary dynamics linked to horizontal gene transfer in vibrios. *Annu. Rev. Microbiol.* **72**, annurev-micro-090817-062148 (2018).

22. Arnold, B. J., Huang, I. T. & Hanage, W. P. Horizontal gene transfer and adaptive evolution in bacteria. *Nature Reviews Microbiology* vol. 20 (2022).

23. Horne, T., Orr, V. T. & Hall, J. P. How do interactions between mobile genetic elements affect horizontal gene transfer? *Curr. Opin. Microbiol.* **73**, 102282 (2023).

24. Bellanger, X., Payot, S., Leblond-Bourget, N. & Guédon, G. Conjugative and mobilizable genomic islands in bacteria: Evolution and diversity. *FEMS Microbiology Reviews* vol. 38 (2014).

25. Khedkar, S. *et al.* Landscape of mobile genetic elements and their antibiotic resistance

cargo in prokaryotic genomes. *Nucleic Acids Res.* **50**, 3155–3168 (2022).

26. Stephens, C. *et al.* F Plasmids Are the Major Carriers of Antibiotic Resistance Genes in Human-Associated Commensal Escherichia coli. *mSphere* **5**, (2020).

27. Alekshun, M. N. & Levy, S. B. Molecular Mechanisms of Antibacterial Multidrug Resistance. *Cell* vol. 128 (2007).

28. Fillol-Salom, A. *et al.* Bacteriophages benefit from mobilizing pathogenicity islands encoding immune systems against competitors. *Cell* **185**, 3248-3262.e20 (2022).

29. Rousset, F. *et al.* Phages and their satellites encode hotspots of antiviral systems. *Cell Host Microbe* **30**, 740-753.e5 (2022).

30. Salomon, D. *et al.* Type VI secretion system toxins horizontally shared between marine bacteria. *PLoS Pathog.* **11**, 1–20 (2015).

31. Jana, B., Keppel, K., Fridman, C. M., Bosis, E. & Salomon, D. Multiple T6SSs, mobile auxiliary modules, and effectors revealed in a systematic analysis of the Vibrio parahaemolyticus pan-genome. *mSystems* e00723-22 (2022) doi:10.1128/MSYSTEMS.00723-22.

32. Thomas, J., Watve, S. S., Ratcliff, W. C. & Hammer, B. K. Horizontal gene transfer of functional type VI killing genes by natural transformation. *MBio* **8**, 1–11 (2017).

33. Santoriello, F. J., Kirchberger, P. C., Boucher, Y. & Pukatzki, S. Pandemic Vibrio cholerae acquired competitive traits from an environmental Vibrio species. *Life Sci. Alliance* **6**, (2023).

34. Ruhe, Z. C., Low, D. A. & Hayes, C. S. Polymorphic toxins and their immunity proteins: Diversity, evolution, and mechanisms of delivery. *Annu. Rev. Microbiol.* **74**, 497–520 (2020).

35. Hurley, C. C., Quirke, A. M., Reen, F. J. & Boyd, E. F. Four genomic islands that mark post-1995 pandemic Vibrio parahaemolyticus isolates. *BMC Genomics* **7**, 104 (2006).

36. Salomon, D. *et al.* Marker for type VI secretion system effectors. *Proc. Natl. Acad. Sci.* **111**, 9271–9276 (2014).

37. Fridman, C. M., Jana, B., Ben-Yaakov, R., Bosis, E. & Salomon, D. A DNase Type VI Secretion System Effector Requires Its MIX Domain for Secretion. *Microbiol. Spectr.* **10**, (2022).

38. Marchler-Bauer, A. *et al.* CDD: a conserved domain database for interactive domain family analysis. *Nucleic Acids Res.* **35**, D237-40 (2007).

39. Zimmermann, L. *et al.* A completely reimplemented MPI bioinformatics toolkit with a new HHpred server at its core. *J. Mol. Biol.* **430**, 2237–2243 (2018).

40. Davidov, E. & Kaufmann, G. RloC: A wobble nucleotide-excising and zinc-responsive bacterial tRNase. *Mol. Microbiol.* **69**, (2008).

41. Shneider, M. M. *et al.* PAAR-repeat proteins sharpen and diversify the type VI secretion system spike. *Nature* **500**, 350–353 (2013).

42. Ray, A. *et al.* Type VI secretion system MIX-effectors carry both antibacterial and anti-eukaryotic activities. *EMBO Rep.* **18**, e201744226 (2017).

43. Dar, Y., Salomon, D. & Bosis, E. The antibacterial and anti-eukaryotic Type VI secretion system MIX-effector repertoire in Vibrionaceae. *Mar. Drugs* **16**, 433 (2018).

44. Jana, B., Fridman, C. M., Bosis, E. & Salomon, D. A modular effector with a DNase domain and a marker for T6SS substrates. *Nat. Commun.* **10**, 3595 (2019).

45. Koskiniemi, S. *et al.* Rhs proteins from diverse bacteria mediate intercellular competition. *Proc. Natl. Acad. Sci. U. S. A.* **110**, 7032–7 (2013).

46. Payne, L. J. *et al.* Identification and classification of antiviral defence systems in bacteria and archaea with PADLOC reveals new system types. *Nucleic Acids Res.* **49**, 10868–10878 (2021).

47. Tesson, F. *et al.* Systematic and quantitative view of the antiviral arsenal of prokaryotes. *Nat. Commun.* **13**, (2022).

48. Maffei, E. *et al.* Systematic exploration of Escherichia coli phage-host interactions with the BASEL phage collection. *PLoS Biol.* **19**, (2021).

49. Knizewski, L., Kinch, L. N., Grishin, N. V, Rychlewski, L. & Ginalski, K. Realm of PD-(D/E)XK nuclease superfamily revisited: detection of novel families with modified transitive meta profile searches. *BMC Struct. Biol.* **7**, 40 (2007).

50. Steczkiewicz, K., Muszewska, A., Knizewski, L., Rychlewski, L. & Ginalski, K. Sequence, structure and functional diversity of PD-(D/E)XK phosphodiesterase superfamily. *Nucleic Acids Res.* **40**, 7016–7045 (2012).

51. Fernández-García, L. & Wood, T. K. Phage-Defense Systems Are Unlikely to Cause Cell Suicide. *Viruses 2023, Vol. 15, Page 1795* **15**, 1795 (2023).

52. Georjon, H. & Bernheim, A. The highly diverse antiphage defence systems of bacteria. *Nature Reviews Microbiology* (2023) doi:10.1038/s41579-023-00934-x.

53. Aframian, N. & Eldar, A. Abortive infection antiphage defense systems: separating mechanism and phenotype. *Trends in Microbiology* vol. 31 1003–1012 (2023).

54. Fernández-García, L. *et al.* Toxin/Antitoxin Systems Induce Persistence and Work in Concert with Restriction/Modification Systems to Inhibit Phage. *bioRxiv* 2023.02.25.529695 (2023) doi:10.1128/SPECTRUM.03388-23.

55. Scherrer, R. & Moyed, H. S. Conditional impairment of cell division and altered lethality in hipA mutants of Escherichia coli K-12. *J. Bacteriol.* **170**, (1988).

56. Granato, E. T., Meiller-Legrand, T. A. & Foster, K. R. The Evolution and Ecology of Bacterial Warfare. *Current Biology* vol. 29 (2019).

57. LeGault, K. N. *et al.* Temporal shifts in antibiotic resistance elements govern phage-pathogen conflicts. *Science.* **373**, (2021).

58. Botelho, J. *et al.* Phylogroup-specific variation shapes the clustering of antimicrobial resistance genes and defence systems across regions of genome plasticity in Pseudomonas aeruginosa. *eBioMedicine* **90**, (2023).

59. Salomon, D. MIX and match: mobile T6SS MIX-effectors enhance bacterial fitness. *Mob. Genet. Elements* **6**, e1123796 (2016).

60. Gibson, D. G. *et al.* Enzymatic assembly of DNA molecules up to several hundred kilobases. *Nat. Methods* **6**, 343–345 (2009).

61. O'Toole, R., Milton, D. L. & Wolf-Watz, H. Chemotactic motility is required for invasion of the host by the fish pathogen Vibrio anguillarum. *Mol. Microbiol.* **19**, 625–637 (1996).

62. Cohen, D. *et al.* Cyclic GMP–AMP signalling protects bacteria against viral infection.

Nature **574**, (2019).

63. Goren, M. G., Mahata, T. & Qimron, U. An efficient, scarless, selection-free technology for phage engineering. *RNA Biol.* **20**, 830–835 (2023).

64. Wannier, T. M. *et al.* Improved bacterial recombineering by parallelized protein discovery. *Proc. Natl. Acad. Sci. U. S. A.* **117**, (2020).

65. Nyerges, Á. *et al.* A highly precise and portable genome engineering method allows comparison of mutational effects across bacterial species. *Proc. Natl. Acad. Sci.* **113**, 2502–2507 (2016).

66. Sharan, S. K., Thomason, L. C., Kuznetsov, S. G. & Court, D. L. Recombineering: a homologous recombination-based method of genetic engineering. *Nat. Protoc. 2009 42* **4**, 206–223 (2009).

67. Yosef, I., Manor, M., Kiro, R. & Qimron, U. Temperate and lytic bacteriophages programmed to sensitize and kill antibiotic-resistant bacteria. *Proc. Natl. Acad. Sci. U. S. A.* **112**, (2015).

68. Kanarek, K., Fridman, C. M., Bosis, E. & Salomon, D. The RIX domain defines a class of polymorphic T6SS effectors and secreted adaptors. *Nat. Commun. 2023 141* **14**, 1–13 (2023).

69. Dar, Y., Jana, B., Bosis, E. & Salomon, D. A binary effector module secreted by a type VI secretion system. *EMBO Rep.* **23**, e53981 (2022).

70. Fridman, C. M., Keppel, K., Gerlic, M., Bosis, E. & Salomon, D. A comparative genomics methodology reveals a widespread family of membrane-disrupting T6SS effectors. *Nat. Commun.* **11**, 1085 (2020).

71. Gabler, F. *et al.* Protein Sequence Analysis Using the MPI Bioinformatics Toolkit. *Curr. Protoc. Bioinforma.* **72**, (2020).

72. Katoh, K., Rozewicki, J. & Yamada, K. D. MAFFT online service: Multiple sequence alignment, interactive sequence choice and visualization. *Brief. Bioinform.* **20**, 1160–1166 (2018).

73. Katoh, K., Misawa, K., Kuma, K. & Miyata, T. MAFFT: a novel method for rapid multiple sequence alignment based on fast Fourier transform. *Nucleic Acids Res.* **30**, 3059–66 (2002).

74. Saitou, N. & Nei, M. The neighbor-joining method: a new method for reconstructing phylogenetic trees. *Mol. Biol. Evol.* **4**, 406–425 (1987).

75. Madeira, F. *et al.* Search and sequence analysis tools services from EMBL-EBI in 2022. *Nucleic Acids Res.* **50**, (2022).

76. Crooks, G. E., Hon, G., Chandonia, J.-M. & Brenner, S. E. WebLogo: a sequence logo generator. *Genome Res.* **14**, 1188–90 (2004).

77. Sievers, F. *et al.* Fast, scalable generation of high-quality protein multiple sequence alignments using Clustal Omega. *Mol. Syst. Biol.* **7**, 539 (2011).

78. Kumar, S., Stecher, G., Li, M., Knyaz, C. & Tamura, K. MEGA X: Molecular evolutionary genetics analysis across computing platforms. *Mol. Biol. Evol.* **35**, 1547–1549 (2018).

79. Robert, X. & Gouet, P. Deciphering key features in protein structures with the new ENDscript server. *Nucleic Acids Res.* **42**, (2014).